

Article

Three-Dimensionally Printed Zero-Valent Copper with Hierarchically Porous Structures as an Efficient Fenton-like Catalyst for Enhanced Degradation of Tetracycline

Sheng Guo ^{1,*} , Meng Chen ², Yao Huang ², Yu Wei ³, Jawad Ali ⁴, Chao Cai ^{3,*} and Qingsong Wei ³

¹ State Key Laboratory of New Textile Materials & Advanced Processing Technologies, Wuhan Textile University, Wuhan 430200, China

² School of Chemistry and Environmental Engineering, Wuhan Institute of Technology, Wuhan 430205, China

³ State Key Laboratory of Materials Processing and Die & Mould Technology, Huazhong University of Science and Technology, Wuhan 430074, China

⁴ School of Environment and Biological Engineering, Wuhan Technology and Business University, Wuhan 430065, China

* Correspondence: guoshengwit@163.com (S.G.); chaocai@hust.edu.cn (C.C.)

Abstract: Three-dimensionally printed materials show great performance and reliable stability in the removal of refractory organic pollutants in Fenton-like reactions. In this work, hierarchically porous zero-valent copper (3DHP-ZVC) was designed and fabricated via 3D printing and applied as a catalyst for the degradation of tetracycline (TC) through heterogeneous Fenton-like processes. It was found that the 3DHP-ZVC/H₂O₂ system could decompose over 93.2% of TC within 60 min, which is much superior to the homogeneous Cu²⁺/H₂O₂ system under similar conditions. The leaching concentration of Cu²⁺ ions in the 3DHP-ZVC/H₂O₂ system is 2.14 times lower than that in the Cu powder/H₂O₂ system in a neutral environment, which could be ascribed to the unique hierarchically porous structure of 3DHP-ZVC. Furthermore, 3DHP-ZVC exhibited compelling stability in 20 consecutive cycles. The effects of co-existing inorganic anions, adaptability, and pH resistance on the degradation of TC were also investigated. A series of experiments and characterizations revealed that Cu⁰ and superoxide radicals as reducing agents could facilitate the cycling of Cu(II)/Cu(I), thus enhancing the generation of hydroxyl radicals to degrade TC. This study provides new insights into employing promising 3D printing technology to develop high-reactivity, stable, and recycling-friendly components for wastewater treatment.

Keywords: 3D print; Fenton; tetracycline; zero valent copper; pollutant degradation



Citation: Guo, S.; Chen, M.; Huang, Y.; Wei, Y.; Ali, J.; Cai, C.; Wei, Q.

Three-Dimensionally Printed Zero-Valent Copper with Hierarchically Porous Structures as an Efficient Fenton-like Catalyst for Enhanced Degradation of

Tetracycline. *Catalysts* **2023**, *13*, 446.

<https://doi.org/10.3390/catal13020446>

Academic Editor: Yat Li

Received: 8 January 2023

Revised: 10 February 2023

Accepted: 17 February 2023

Published: 19 February 2023



Copyright: © 2023 by the authors. Licensee MDPI, Basel, Switzerland. This article is an open access article distributed under the terms and conditions of the Creative Commons Attribution (CC BY) license (<https://creativecommons.org/licenses/by/4.0/>).

1. Introduction

Antibiotics are chemical medicines that possess antibacterial activity and are widely employed for the treatment of bacterial infections [1–5]. Recently, antibiotics have been extensively detected in aquatic systems owing to the overuse of antibiotics and the incomplete metabolism of humans and animals [6,7]. The long-term accumulation of antibiotics in water bodies may increase antibiotic resistance, which seriously threatens human health [8–10]. Conventional techniques such as adsorption, biological treatment, and membrane separation are limited by their low and insufficient removal efficiency [11]. Therefore, the development of an economic and efficient route for antibiotic elimination is urgently needed.

Fenton processes are frequently applied to decompose hazardous organic pollutants, which can produce highly oxidized hydroxyl radicals ([•]OH) (1.9–2.7 V vs. NHE) through the catalytic decomposition of hydrogen peroxide (H₂O₂) by Fe²⁺ or other transition metals [12–15]. However, the practical application of the conventional Fenton reaction is hindered by iron-sludge generation, the impossibility of recycling, and a narrow operational pH range [16]. Heterogeneous Fenton or Fenton-like catalysts have received

increasing attention, which greatly overcome the above drawbacks of conventional Fenton reactions [17–20]. Among various developed heterogeneous catalysts, zero-valent copper (ZVC) arouses ever-growing interest due to its unique merits of excellent electrical conductivity and high stability. As reported, ZVC frequently serves as an intermediate of electronic transmission, which is responsible for the better activation of H_2O_2 [21]. In addition, ZVC demonstrates more reliable stability than zero-valent iron (ZVI) owing to the drawbacks of easy agglomeration and oxidation nature [22]. To date, a series of ZVC catalysts have been synthesized due to these advantages, but they are generally in the form of nanoparticles, which is inconvenient in separation and recovery from an aqueous environment, raising the risk of secondary contamination [23]. It is desired to break through the rigid concepts of nanoparticles to manufacture stable, high-reactivity, and recycling-friendly catalysts via a feasible method for practical application.

Three-dimensional (3D) printing technology is an additive manufacturing process used to manufacture specialized functional structures directly guided by a 3D model, which greatly optimizes structural properties and simplifies manufacturing processes, further minimizing production costs [24]. Three-dimensional printing technology is highly appropriate in the field of catalysis owing to its distinctive functional structures and favorable control of the target catalysts, which is of vital significance for the performance of catalytic materials [25]. Among the multifarious 3D printing techniques, selective laser melting (SLM) is a preferred technology to fabricate metallic components with sufficient accuracy to lattice structures from powder [26]. Recent studies have indicated that SLM-produced catalysts act as effective and stable activators for H_2O_2 . For example, Yang et al. designed a hierarchical porous metallic glass/copper composite to activate H_2O_2 for wastewater treatment, with a rate constant of removing rhodamine B (RhB) 620 times higher than commercial zero-valent iron particles [27]. In our previous work, hierarchically micro- and nanoporous Cu catalysts were prepared for H_2O_2 activation through the combination of SLM and chemical dealloying techniques [28]. However, the obtained Cu catalysts encounter the dilemmas of having a complicated process, high dissolution, and excessive oxidant consumption.

In this work, ZVC with hierarchically porous structures (3DHP-ZVC) was fabricated as an efficient Fenton-like catalyst to decompose multiple organic pollutants via 3D printing technology, which displayed excellent reactivity for H_2O_2 activation. The morphology, catalytic performance, stability, and universality of the printed 3DHP-ZVC were thoroughly illustrated. The influence of essential factors such as initial pH, H_2O_2 concentration, and co-existing inorganic anions was evaluated. Finally, a possible activation mechanism was proposed and confirmed by experiments and characterization analysis. Our study provides a novel strategy to develop stable and recycling-friendly catalysts in Fenton-like systems for wastewater purification.

2. Results and Discussion

2.1. Characterization

The X-ray diffraction (XRD) patterns of the printed 3DHP-ZVC are presented in Figure 1a. The characteristic peaks at 2θ of 43.3° , 50.4° , 74.1° , 89.9° , and 95.1° could be ascribed to the (111), (200), (220), (311), and (222) lattice planes of Cu^0 (PDF#04–0836), respectively [29]. This result indicated that the developed 3DHP-ZVC samples were composed of Cu^0 . X-ray photoelectron spectroscopy (XPS) provides available element information on the surface of 3DHP-ZVC. As depicted in Figure 1b, Cu 2p peaks located at 931.8 and 951.6 eV were consistent with the binding energies of Cu^0 [30,31]. Meanwhile, the relatively weak peaks at 934.2, 954.2, and 941.6 eV were ascribed to the appearance of a trace amount of Cu^{2+} due to the inevitable surface oxidation during the XPS determination [31]. Similar phenomena that the characteristic peaks of Cu^{2+} were also detected on the surface of Cu^0 in XPS measurements were observed in previous studies [32]. The surface images of the 3DHP-ZVC samples were revealed using a scanning electron microscopy (SEM) instrument (Figure 1c–f). 3DHP-ZVC possesses hierarchically porous structures and a

coarse surface, which is beneficial to the exposure of more active sites (Figure 1c) [33]. Moreover, Brunauer–Emmett–Teller (BET) analysis was applied to measure the specific surface area of the samples. The surface area of 3DHP-ZVC ($2.5 \text{ m}^2/\text{g}$) is comparable to that of Cu powder ($3.1 \text{ m}^2/\text{g}$), suggesting that the specific surface area characteristic undergoes no significant change during the printing process.

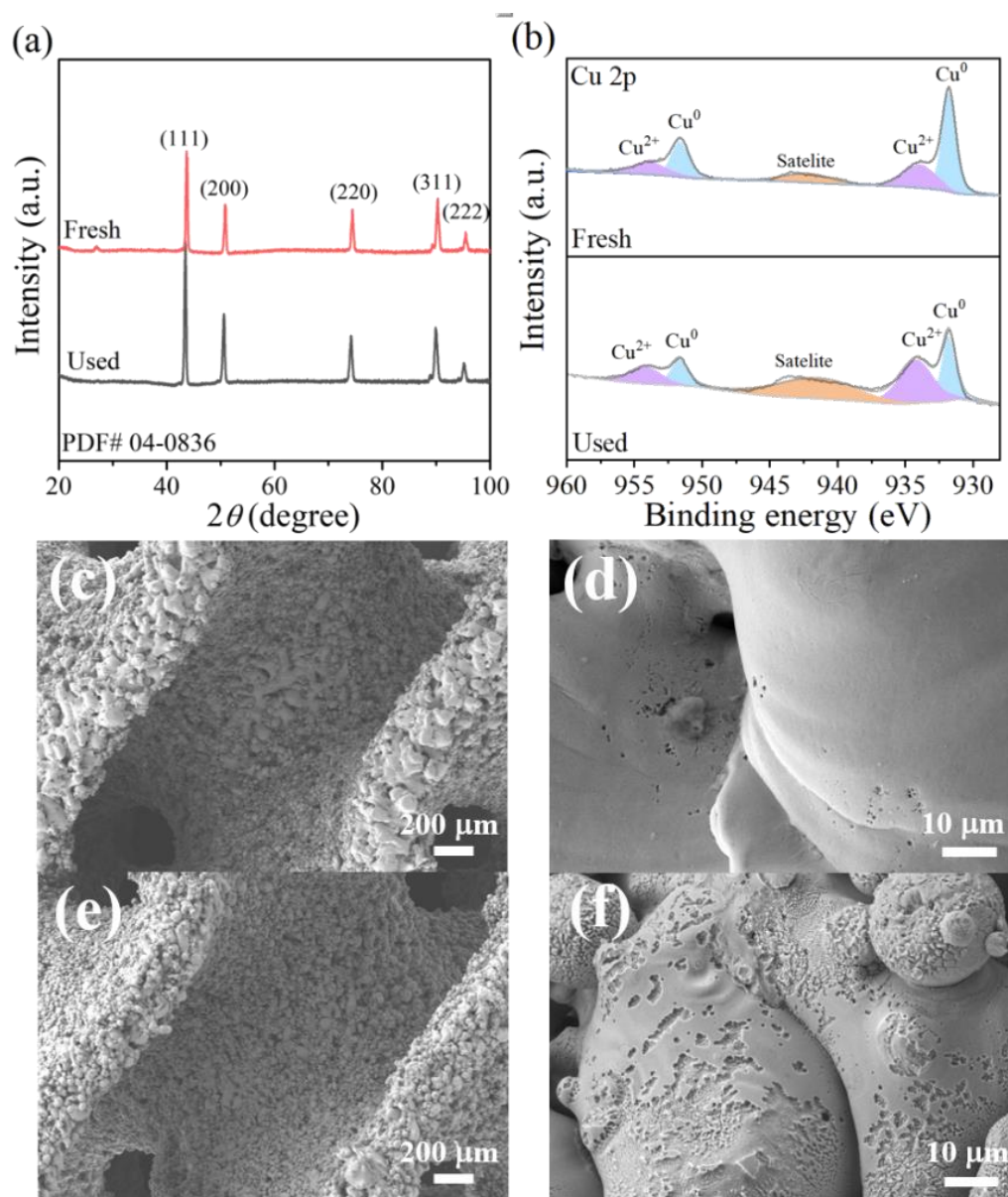


Figure 1. (a) XRD patterns of 3DHP-ZVC, (b) Cu 2p XPS spectra of 3DHP-ZVC before and after reactions, and SEM images of (c,d) 3DHP-ZVC, and (e,f) used 3DHP-ZVC.

2.2. Catalytic Performance of 3DHP-ZVC

The Fenton-like performance of the developed 3DHP-ZVC samples was evaluated using tetracycline (TC, a typical antibiotic) as a target pollutant. As presented in Figure 2a,b, H_2O_2 decomposed a negligible amount of TC, while 40.8% of TC was removed by sole 3DHP-ZVC within 60 min. Nevertheless, the removal efficiency of TC was remarkably improved to 93.2% in the 3DHP-ZVC/ H_2O_2 system. Furthermore, the concentration of Cu^{2+} ions was determined to be 0.7 mg/L during the reaction process under a neutral condition, which was much lower than the permissible limit of the World Health Organization (2 mg/L) [34]. The homogeneous leaching copper ions contributed only 13.5%

of TC degradation with the addition of H_2O_2 , suggesting the removal of TC was mainly invoked via a heterogeneous catalytic reaction of 3DHP-ZVC. Figure 2b presents the comparison of different catalyst- H_2O_2 systems under neutral conditions. Although the form of powder was easily dispersed in the solution, the aggregation of Cu powder would inevitably prevent contact among H_2O_2 and TC molecules, resulting in comparable catalytic performance to 3DHP-ZVC. However, the leaching concentration of Cu^{2+} ions in the Cu powder/ H_2O_2 system (1.5 mg/L) was 2.14 times that in the 3DHP-ZVC/ H_2O_2 system (0.7 mg/L), implying the merit of the hierarchically porous structures.

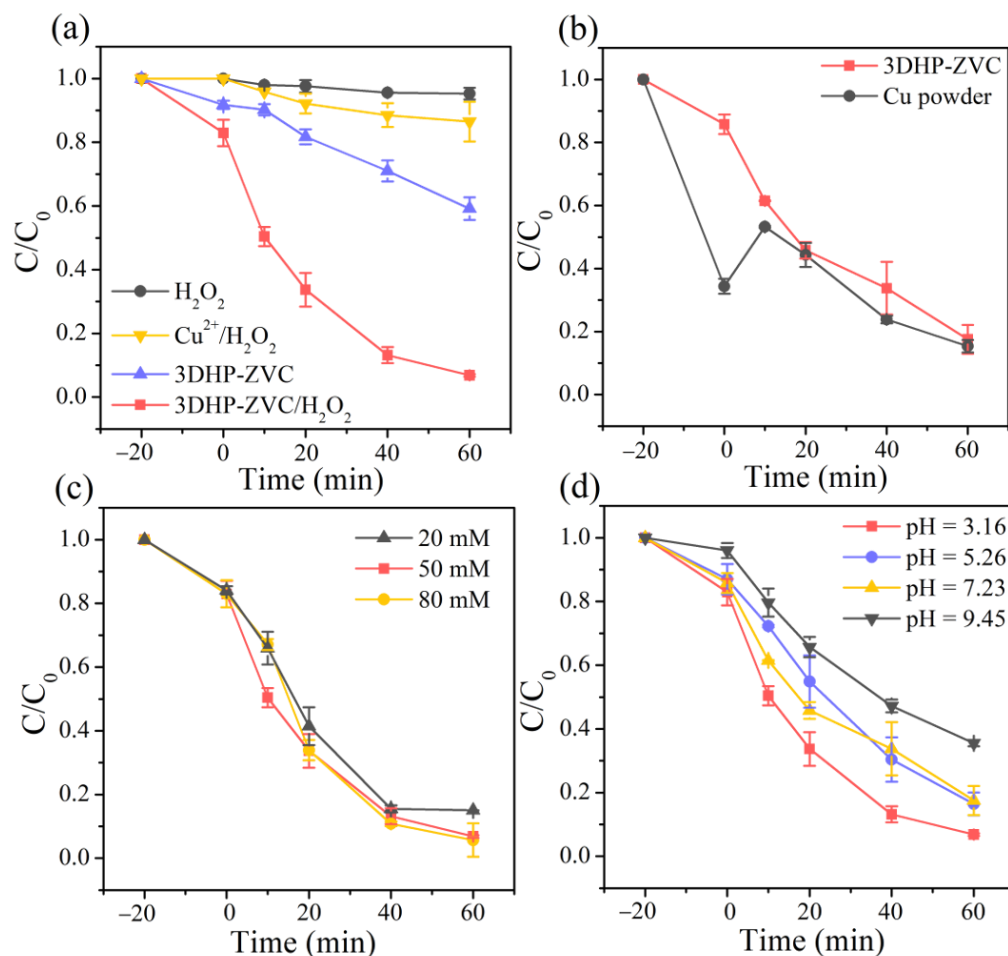


Figure 2. TC degradation (a) in different systems under optimal conditions, (b) by different catalyst- H_2O_2 systems at pH = 7.23, effects of (c) H_2O_2 dosage, and (d) initial pH value on the degradation of TC.

The concentration of the leaching metal ions was measured to be approximately 10 mg/L in the ZVI/ H_2O_2 system under identical conditions, which was 14.3 times higher than that of the 3DHP-ZVC/ H_2O_2 system. These results indicate the excellent catalytic activity and reliable stability of 3DHP-ZVC in activating H_2O_2 . Furthermore, 3DHP-ZVC exhibits comparable catalytic performance in activating H_2O_2 and demonstrates better recycling performance compared to those of many other Cu-based catalysts (Table 1).

Table 1. Comparison of catalytic activity of various Cu-based catalysts in references.

Catalyst	H ₂ O ₂ Concentration (mM)	Pollutant Concentration (mg/L)	Removal Efficiency	Cycle Number	Reference
CuNx	80	TC 20	93.6% (60 min)	5	[35]
CuxNiyCo-LDH/GO	10	TC 20	96.5% (40 min)	5	[36]
CuFeO QDs/CNNSs	100	TC 50	99.8% (25 min)	5	[37]
CuS@GCS ENFC	67	TC 10	81.3 (120 min)	4	[38]
ZVC	10	Norfloxacin 5	46.7% (30 min)	Not available	[39]
NPC@DCS (Cu)	500	RhB 10	100% (60 min)	5	[28]
nZVC-Cu(II)-rGO	10	2-chlorophenol 10	91.8% (60 min)	8	[40]
3DHP-ZVC	50	TC 10	93.2 % (60 min)	20	This work

2.3. Influence of Experimental Conditions

2.3.1. Effect of H₂O₂ Concentration

The concentration of H₂O₂ can significantly affect the degradation of TC in the 3DHP-ZVC/H₂O₂ system. As illustrated in Figure 2c, the decomposition of TC was enhanced by raising the H₂O₂ concentration from 20 to 50 mM, which was attributed to the generation of more active radicals [41]. Nevertheless, further increasing the H₂O₂ amount to 80 mM did not significantly improve the TC removal owing to the radical scavenging effect of excessive H₂O₂ [42]. Thus, the optimal H₂O₂ dosage was fixed at 50 mM.

2.3.2. Effect of Initial pH

The initial pH of the solution plays an essential role during Fenton-like processes [43]. Therefore, various experiments were performed over a pH range from 3.16 to 9.45 to investigate the catalytic activity of the 3DHP-ZVC/H₂O₂ system. As illustrated in Figure 2d, the highest degradation efficiency of TC reached 93.2% at pH = 3.16 and slightly decreased to 83.5% and 82.4% with increasing pH to 5.25 and 7.23, respectively. Such an observation might be ascribed to the fact that more active intermediates were released under acidic conditions [44]. However, when the solution pH was further raised to 9.45, the degradation activity significantly decreased, which was assigned to a decreased redox potential of •OH and the appearance of Cu(OH)₂ [45,46]. Moreover, an alkaline environment favors the existence of more carbonate and bicarbonate, which are typical •OH quenches [45]. It is noted that the efficient degradation efficiency was maintained at over 82% under acidic and neutral pH conditions (3.16–7.23), implying its great potential for practical application.

2.4. Environmental Applications

Inorganic anions, widespread in actual water environments, are capable of competing for possible reactive oxygen species with target pollutants, which shows their significant impact on the oxidation process [47,48]. As revealed in Figure 3a, the addition of HCO₃[−] and HPO₄^{2−} to the reaction drastically delayed the removal efficiency of TC from 93.2% to 75.3% and 72.4%, respectively, which was attributed to the scavenging effect of HCO₃[−] and HPO₄^{2−} for •OH [49]. Comparatively, SO₄^{2−} and NO₃[−] exhibited a negligible inhibitory effect in the process owing to the slow reaction with reactive oxygen species, which was consistent with previous reports [50]. In contrast, adding 10 mM of Cl[−] to the reaction

solution significantly promoted the decomposition of TC due to the formation of various chlorine active species in the reaction, such as $\text{Cl}^{\bullet-}$, $\text{ClOH}^{\bullet-}$, and $\text{Cl}_2^{\bullet-}$ [51].

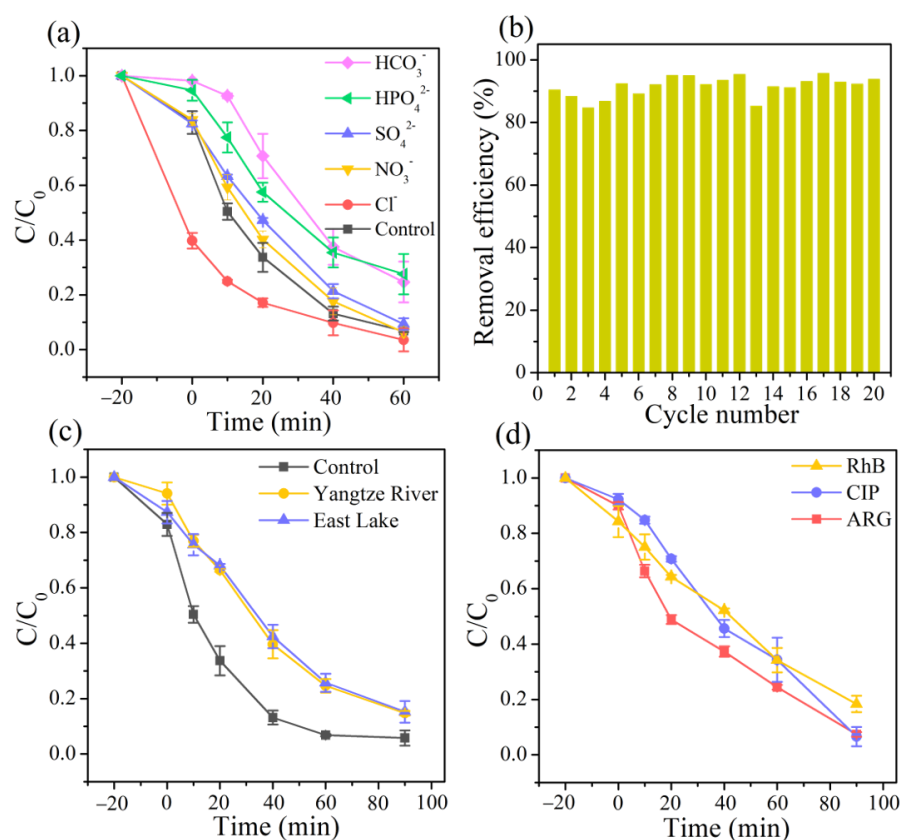


Figure 3. (a) Effects of co-existing inorganic anions (10 mM), (b) the reusability of the 3DHP-ZVC samples, (c) various water systems on the TC removal, and (d) degradation of different organic pollutants including RhB, CIP, and ARG.

The stability of the obtained 3DHP-ZVC samples was also evaluated. As displayed in Figure 3b, the catalytic activity of 3DHP-ZVC for TC degradation had no significant decay during 20 continuous cycles, which exceeds most of the conventional Cu-based nanoparticle catalysts. This result may be due to the advantages of hierarchically porous structures of 3DHP-ZVC, which facilitate separation and recovery from water bodies and reduce the dissolution of ions, decreasing the risk of secondary pollution. In addition, no change had been observed in the XRD spectra of the 3DHP-ZVC sample after the reaction process, indicating its excellent structural stability (Figure 1a).

To explore the adaptation of 3DHP-ZVC for further practical applications, the reactions in different actual water matrixes were conducted and the catalytic performance toward various organic contaminants was investigated. The removal efficiency of TC achieved 85.3% and 84.7% in the Yangtze River and East Lake water, respectively, implying the great application potential of 3DHP-ZVC in actual water treatment (Figure 3c). In addition, RhB (a cationic dye), ciprofloxacin (CIP, an antibiotic), and acid red G (ARG, an azo dye) were selected to prove the applicability of the 3DHP-ZVC/ H_2O_2 system. Figure 3d demonstrates that all the selected contaminants could be decomposed by over 82% in 90 min, indicating that 3DHP-ZVC is potentially effective in Fenton-like systems for wastewater purification.

2.5. Activation Mechanism

Numerous studies have confirmed that $\bullet\text{OH}$ and superoxide radicals ($\text{O}_2^{\bullet-}$) play essential roles in heterogeneous Fenton systems [52–54]. Therefore, tert-butanol (TBA, a typical scavenger for $\bullet\text{OH}$) and chloroform (CHCl_3 , an effective scavenger of $\text{O}_2^{\bullet-}$) were

used to investigate the contribution of $\bullet\text{OH}$ and $\text{O}_2^{\bullet-}$ radicals in the 3DHP-ZVC/ H_2O_2 system [41,55]. As shown in Figure 4a, adding 1 M of TBA to the reaction solution dropped the degradation efficiency of TC from 93.2% to 32.9% within 60 min and significantly suppressed it to 21.4% with the TBA concentration further increasing to 3 M. Meanwhile, the reaction rate in the existence of TBA (3 M) was dramatically decreased over 13 times compared to the control groups (Figure 4c). These results indicated the dominant role of $\bullet\text{OH}$ in the 3DHP-ZVC/ H_2O_2 system. The introduction of 0.1–0.3 M of CHCl_3 resulted in a significant inhibition effect on the TC removal, suggesting that $\text{O}_2^{\bullet-}$ also participated in the reaction. Recent reports indicate that the cycle of Cu(II)/Cu(I) is responsible for the generation of $\bullet\text{OH}$ for TC degradation [56]. To ascertain this conclusion, neocuproine (NCP) and ethylene diamine tetraacetic acid (EDTA) were employed to identify the role of Cu(I) and Cu(II) during the reaction, respectively [57]. As shown in Figure 4b,d, the presence of NCP and EDTA greatly prevented the removal of TC, strongly confirming the involvement of Cu(I) and Cu(II) in the reaction. In addition, it is widely accepted that the reduction of high-valent species is the rate-limiting step in the oxidation process. Hydroxylamine (HA) served as a reducing agent that significantly accelerated the degradation of TC (Figure 4b,d), indicating the cycle of Cu(II)/Cu(I) [58]. Besides, compared to fresh 3DHP-ZVC, the relative ratio of Cu^{2+} and Cu^0 (Figure 1b) increased significantly for the used 3DHP-ZVC samples, and slight corrosion was observed after the oxidation process (Figure 1e,f), which elucidated the transformation of Cu^0 to Cu^{2+} in the TC degradation process.

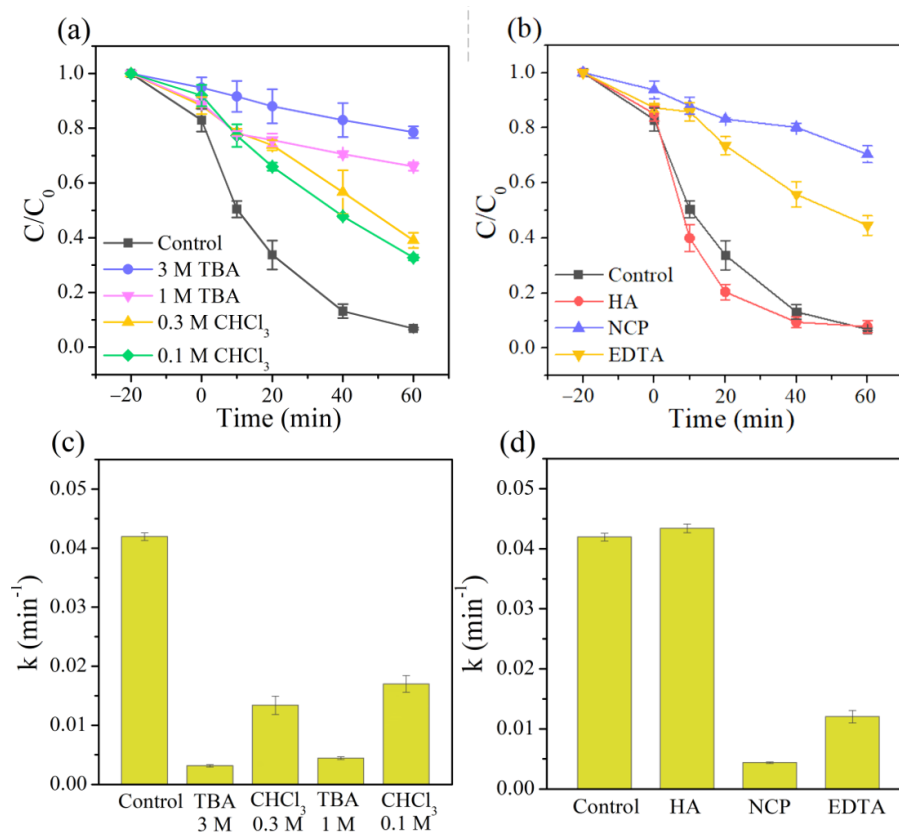
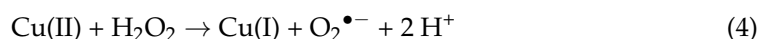
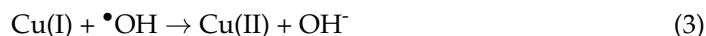
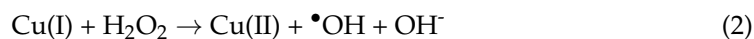
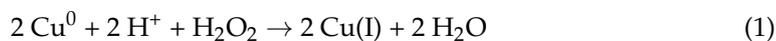


Figure 4. Effects of (a) different scavengers (TBA and CHCl_3), (b) HA, NCP, and EDTA for TC removal in the 3DHP-ZVC/ H_2O_2 system, and (c,d) their corresponding reaction rate constant under different conditions.

According to the above discussion, a feasible mechanism for TC removal in the 3DHP-ZVC/ H_2O_2 system was proposed. First, the surface of 3DHP-ZVC was corroded by H^+ and H_2O_2 to release Cu(I) (Equation (1)) [59]. The released Cu(I) was responsible for the H_2O_2 activation to generate $\bullet\text{OH}$, as described by Equation (2) [60]. Subsequently, Cu(I) was further oxidized by $\bullet\text{OH}$ to generate Cu(II), and $\text{O}_2^{\bullet-}$ was produced with the reaction

between Cu(II) and H₂O₂ (Equations (3) and (4)) [61,62]. Then, O₂^{•-} and Cu⁰ could serve as reducing agents for the regeneration of Cu(I) via Equations (5) and (6) [62,63]. Finally, the removal of TC was achieved by the generation of [•]OH in the 3DHP-ZVC/H₂O₂ system.



2.6. Analysis of TC Removal by 3D-EEMs

Three-dimensional excitation-emission matrix fluorescence spectroscopy (EEMS) technology was applied to explain the overall removal and mineralization of TC in the 3DHP-ZVC/H₂O₂ system. As revealed in Figure 5a, no fluorescence peak was observed in the initial TC solution due to the electron-withdrawing groups of TC, which was consistent with previous reports [64]. Two maxima fluorescence peaks belonging to the areas of fulvic acids-like ($E_x/E_m = 260\text{--}320/400\text{--}460$) and humic acid ($E_x/E_m = 300\text{--}360/460\text{--}550$) were found after degradation for 30 min (Figure 5b) [65]. When the degradation time was increased to 60 min, the intensities of the fluorescence signals were significantly weakened, and the signals disappeared when increasing the reaction time to 24 h, implying that the generated intermediate substances were finally mineralized into smaller fragments (Figure 5c,d). The change in the intensity of fluorescence signals during the reaction reflects the removal pathway of TC to some extent.

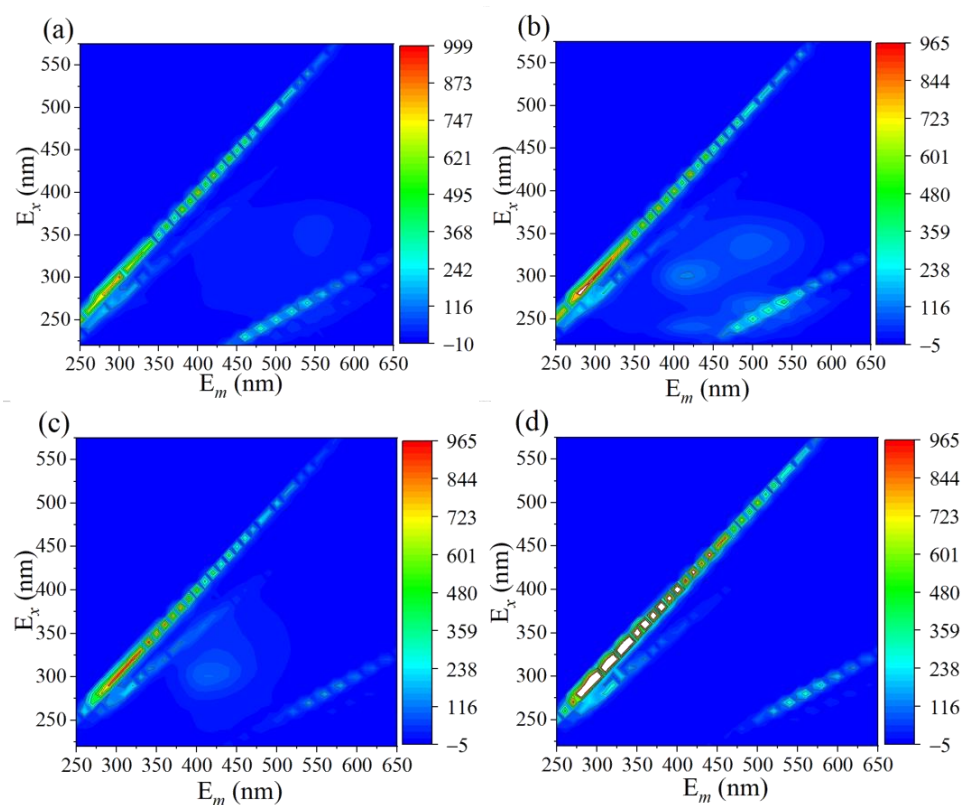


Figure 5. Three-dimensional EEM fluorescence spectra of TC solution after (a) 0 min, (b) 30 min, (c) 60 min, and (d) 24 h during the reaction.

3. Materials and Methods

3.1. Materials and Reagents

NaOH, HNO₃, RhB, H₂O₂, HA, EDTA, Na₂HPO₄, NaCl, Na₂SO₄, NaHCO₃, NaNO₃, and CHCl₃ were purchased from China Sinopharm Chemical Reagent Co., Ltd. (Shanghai, China). TBA, NCP, and TC were supplied by China Aladdin Chemistry Co., Ltd. (Shanghai, China). ARG and CIP were obtained from China Macklin in Biochemical Reagent Co., Ltd. (Shanghai, China). All reagents used in this experiment were analytical grade and used without further purification. Pure copper powder was supplied from VilWory Advanced Materials Technology Co., Ltd. (Jiangsu, China).

3.2. SLM Processing

Cu powder particles (15–40 μm) with spherical shapes were sieved out for SLM processing. The samples were fabricated through a self-developed SLM-150 machine (ZRRapid Tech, Suzhou, China), where a 500 W fiber laser was equipped. The chamber was full of high-purity argon to prevent oxygen. The laser scanning speed and power play a vital role in the quality of the SLM-produced samples [66]. To minimize the possible defects, the optimized parameters are listed in Table 2, and the SLM process is illustrated in Figure 6.

Table 2. Optimized parameters in this work and the weight and dimension of 3DHP-ZVC.

Scanning Speed (mm/s)	Laser Power (W)	Layer Thickness (mm)	Hatch Spacing (mm)	Weight (g)	Dimension (mm × mm × mm)
600	300	0.03	0.10	2.1	10 × 10 × 10

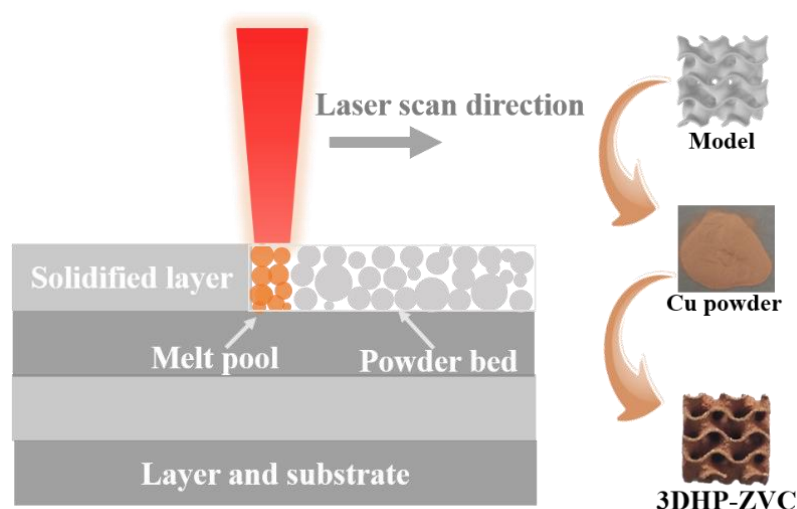


Figure 6. Schematic illustration of printing 3DHP-ZVC through SLM technology.

3.3. Characterization

The microstructure of the 3DHP-ZVC catalysts was characterized via X-ray diffraction (XRD, XRD 6100, Kratos, Kyoto, Japan), and the data were determined from 20° to 100°. The surface morphology information was obtained via Scanning Electron Microscopy (SEM, Gemini 300, ZEISS, Oberkochen, Germany). The chemical state of the fresh and used 3DHP-ZVC was determined using an X-ray photoelectron spectroscopy (XPS, ESCALAB XI+, Thermo, Waltham, MA, USA) instrument. Three-dimensional excitation-emission matrix fluorescence spectra (3D EEMs, F-2700, HITACHI, Tokyo, Japan) were used to investigate the degradation pathway of TC. The leached Cu²⁺ ions were obtained through an SP-3520AA atomic absorption spectrometer (SP-3520AA, Shanghai Spectrum Instruments, Shanghai, China). The specific surface area of the samples was measured through

nitrogen adsorption on an ASAP2020 HD88 nitrogen adsorption apparatus (Micromeritics, Shanghai, China).

3.4. Experimental Procedure

All the degradation reactions were performed in 250 mL glass beakers in a water bath under continuous magnetic stirring. Firstly, 2.1 g of 3DHP-ZVC was sunk into 100 mL of TC reaction solution (10 mg/L) for 30 min to achieve an adsorption equilibrium. The reaction was initiated by the addition of a certain amount of H₂O₂. At fixed intervals, the reaction solution (approximately 2 mL) was taken out for immediate measurement using a UV–vis spectrophotometer (UV–1990PC, AOE Instruments, Shanghai, China). The maximum detection wavelength of ARG, RhB, CIP, and TC was 505, 554, 275, and 356 nm, respectively. In typical experiments, the dosage of H₂O₂ was 50 mM, and the solution of initial pH was adjusted to 3 unless otherwise stated. NaOH or HNO₃ solution (0.1 M) was applied to adjust the pH of the TC solution. After each cycle, the 3DHP-ZVC catalyst was extracted from the solution and rinsed using an ultrasonic cleaning instrument (KM-400KDE, Meimei Ultrasonic Instrument Co., Ltd., Kunshan, China) with deionized water for 30 min.

4. Conclusions

In summary, a novel 3DHP-ZVC catalyst with hierarchically porous structures was developed via 3D printing technology and served as an efficient H₂O₂ activator to decompose various organic pollutants (e.g., TC, RhB, CIP, and ARG). The obtained hierarchically porous 3DHP-ZVC samples not only facilitated recycling but reduced ionic leaching compared to Cu powder particles for H₂O₂ activation to remove TC. Under optimal conditions, the 3DHP-ZVC/H₂O₂ system could remove over 93.2% of TC, which is much superior to the homogeneous Cu²⁺/H₂O₂ system. The catalyst presented excellent stability for 20 continuous cycles without significant decay. In addition, the 3DHP-ZVC/H₂O₂ system demonstrated general applicability under a pH range from 3.16 to 7.23 and actual water environments. Trapping experiments indicated that •OH radicals were the dominant active species and O₂•[−] were involved in the 3DHP-ZVC/H₂O₂ system. The cycle of Cu(II)/Cu(I) was proved to be responsible for the generation of •OH and O₂•[−]. This work paves a new avenue to the development of stable and recycling-friendly catalysts in Fenton-like systems for environmental remediation.

Author Contributions: Conceptualization, S.G.; funding acquisition, S.G. and C.C.; formal analysis, Y.H.; investigation, Y.W., Q.W. and J.A.; project administration, S.G.; supervision, S.G. and C.C.; software, Y.W. and J.A.; validation, C.C. and Q.W.; visualization, M.C. and Y.H.; writing—original draft preparation, M.C.; writing—review and editing, S.G. All authors have read and agreed to the published version of the manuscript.

Funding: This work received financial support from the National Natural Science Foundation of China (Nos. 51604194 and 51905192) and the Natural Science Foundation of Hubei Province of China (No. 2021CFB296).

Data Availability Statement: The data presented in this study are openly available.

Conflicts of Interest: The authors declare no conflict of interest.

References

1. Gao, Y.W.; Zhu, Y.; Li, T.; Chen, Z.H.; Jiang, Q.K.; Zhao, Z.Y.; Liang, X.Y.; Hu, C. Unraveling the high-activity origin of single-atom iron catalysts for organic pollutant oxidation via peroxymonosulfate activation. *Environ. Sci. Technol.* **2021**, *55*, 8318–8328. [[CrossRef](#)] [[PubMed](#)]
2. Liu, X.L.; Pang, H.W.; Liu, X.W.; Li, Q.; Zhang, N.; Mao, L.; Qiu, M.Q.; Hu, B.W.; Yang, H.; Wang, X.K. Orderly porous covalent organic frameworks-based materials: Superior adsorbents for pollutants removal from aqueous solutions. *Innovation* **2021**, *2*, 100076. [[CrossRef](#)] [[PubMed](#)]
3. Kouvelis, K.; Kampioti, A.A.; Petala, A.; Frontistis, Z. Degradation of sulfamethoxazole using a hybrid CuO_x-BiVO₄/SPS/solar system. *Catalysts* **2022**, *12*, 882. [[CrossRef](#)]

4. Chen, Z.; Wei, W.; Chen, H.; Ni, B.J. Recent advances in waste-derived functional materials for wastewater remediation. *EEH* **2022**, *1*, 86–104. [[CrossRef](#)]
5. Wang, T.Z.; Cao, X.J.; Jiao, L.F. Ni₂P/NiMoP heterostructure as a bifunctional electrocatalyst for energy-saving hydrogen production. *EScience* **2021**, *1*, 69–74. [[CrossRef](#)]
6. Zhu, L.L.; Ji, J.H.; Liu, J.; Mine, S.Y.; Matsuoka, M.Y.; Zhang, J.L.; Xing, M.Y. Designing 3D-MoS₂ sponge as excellent cocatalysts in advanced oxidation processes for pollutant control. *Angew. Chem. Int. Ed.* **2020**, *132*, 14072–14080. [[CrossRef](#)]
7. Zhang, X.K.; Liu, J.H.; Zheng, X.C.; Chen, R.; Zhang, M.; Liu, Z.Y.; Wang, Z.Y.; Li, J. Activation of oxalic acid via dual-pathway over single-atom Fe catalysts: Mechanism and membrane application. *Appl. Catal. B—Environ.* **2023**, *321*, 122068. [[CrossRef](#)]
8. Yin, H.L.; Cai, Y.W.; Li, G.Y.; Wang, W.J.; Wong, P.K.; An, T.C. Persistence and environmental geochemistry transformation of antibiotic-resistance bacteria/genes in water at the interface of natural minerals with light irradiation. *Crit. Rev. Environ. Sci. Technol.* **2022**, *52*, 2270–2301. [[CrossRef](#)]
9. Qin, D.Y.; Zhang, C.; Zhou, Y.; Qin, F.Z.; Wang, H.; Wang, W.J.; Yang, Y.; Zeng, G.M. Dual optimization approach to Mo single atom dispersed g-C₃N₄ photocatalyst: Morphology and defect evolution. *Appl. Catal. B—Environ.* **2022**, *303*, 120904.
10. Li, C.Q.; Huang, Y.; Dong, X.B.; Sun, Z.M.; Duan, X.D.; Ren, B.X.; Zheng, S.L.; Dionysiou, D.D. Highly efficient activation of peroxymonosulfate by natural negatively-charged kaolinite with abundant hydroxyl groups for the degradation of atrazine. *Appl. Catal. B—Environ.* **2019**, *247*, 10–23. [[CrossRef](#)]
11. Chen, G.Y.; Yu, Y.; Liang, L.; Duan, X.G.; Li, R.; Lu, X.K.; Yan, B.B.; Li, N.; Wang, S.B. Remediation of antibiotic wastewater by coupled photocatalytic and persulfate oxidation system: A critical review. *J. Hazard. Mater.* **2021**, *408*, 124461. [[CrossRef](#)]
12. Chen, F.X.; Lv, H.X.; Chen, W.; Chen, R. Catalytic wet peroxide oxidation of anionic pollutants over fluorinated Fe₃O₄ microspheres at circumneutral pH values. *Catalysts* **2022**, *12*, 1564. [[CrossRef](#)]
13. Yang, Z.X.; Wang, Z.Z.; Wang, J.T.; Li, Y.; Zhang, G.K. Facet-dependent activation of oxalic acid over magnetic recyclable Fe₃S₄ for efficient pollutant removal under visible light irradiation: Enhanced catalytic activity, DFT calculations, and mechanism insight. *Environ. Sci. Technol.* **2022**, *56*, 18008–18017. [[CrossRef](#)]
14. Van Scoy, A.R.; Tjeerdema, R.S. Environmental fate and toxicology of chlorothalonil. *Rev. Environ. Contam. Toxicol.* **2014**, *232*, 89–105.
15. Tian, X.K.; Gao, P.P.; Nie, Y.L.; Yang, C.; Zhou, Z.X.; Li, Y.; Wang, Y.X. A novel singlet oxygen involved peroxymonosulfate activation mechanism for degradation of ofloxacin and phenol in water. *Chem. Commun.* **2017**, *53*, 6589–6592. [[CrossRef](#)]
16. Guo, S.; Yang, W.; You, L.M.; Li, J.; Chen, J.Y.; Zhou, K. Simultaneous reduction of Cr(VI) and degradation of tetracycline hydrochloride by a novel iron-modified rectorite composite through heterogeneous photo-Fenton processes. *Chem. Eng. J.* **2020**, *393*, 124758. [[CrossRef](#)]
17. Kaushal, S.; Singh, P.P.; Kaur, N. Metal organic framework-derived Zr/Cu bimetallic photocatalyst for the degradation of tetracycline and organic dyes. *Environ. Nanotechnol. Monit. Manag. Environ.* **2022**, *18*, 100727. [[CrossRef](#)]
18. Jawad, A.; Chen, Z.Q.; Yin, G.C. Bicarbonate activation of hydrogen peroxide: A new emerging technology for wastewater treatment. *Chin. J. Catal.* **2016**, *37*, 810–825. [[CrossRef](#)]
19. Su, C.P.; Cheng, M.X.; Tian, F.; Chen, F.X.; Chen, R. Anti-oil-fouling Au/BiOCl coating for visible light-driven photocatalytic inactivation of bacteria. *J. Colloid Interface Sci.* **2022**, *628*, 955–967. [[CrossRef](#)]
20. Wu, X.; Zhang, W.L.; Li, J.; Xiang, Q.J.; Liu, Z.Y.; Liu, B. Identification of the active sites on metallic MoO_{2-x} nano-sea-urchin for atmospheric CO₂ photoreduction under UV, visible, and near-infrared light illumination. *Angew. Chem. Int. Ed.* **2022**, *62*, e202213124.
21. Zarif, F.; Khurshid, S.; Muhammad, N.; Qureshi, M.Z.; Shah, N.S. Colorimetric sensing of hydrogen peroxide using ionic-liquid-sensitized zero-valent copper nanoparticle (nZVCu). *Chem. Sel.* **2020**, *5*, 6066–6074. [[CrossRef](#)]
22. Li, C.Q.; Yang, S.S.; Bian, R.Z.; Tan, Y.; Zhang, X.W.; Zheng, S.L.; Sun, Z.M. Efficient catalytic degradation of bisphenol A coordinated with peroxymonosulfate via anchoring monodispersed zero-valent iron on natural kaolinite. *Chem. Eng. J.* **2022**, *448*, 137746. [[CrossRef](#)]
23. Rajput, V.; Minkina, T.; Ahmed, B.; Sushkova, S.; Singh, R.; Soldatov, M.; Laratte, B.; Fedorenko, A.; Mandzhieva, S.; Blicharska, E.; et al. Interaction of copper-based nanoparticles to soil, terrestrial, and aquatic systems: Critical review of the state of the science and future perspectives. *Rev. Environ. Contam. Toxicol.* **2019**, *252*, 51–96.
24. Guo, S.; Chen, M.; You, L.M.; Wei, Y.; Cai, C.; Wei, Q.S.; Zhang, H.L.; Zhou, K. 3D printed hierarchically porous zero-valent copper for efficient pollutant degradation through peroxymonosulfate activation. *Sep. Purif. Technol.* **2023**, *305*, 122437. [[CrossRef](#)]
25. Zhou, X.T.; Liu, C.J. Three-dimensional printing for catalytic applications: Current status and perspectives. *Adv. Funct. Mater.* **2017**, *27*, 1701134. [[CrossRef](#)]
26. Maconachie, T.; Leary, M.; Lozanovski, B.; Zhang, X.Z.; Qian, M.; Faruque, Q.; Brandt, M. SLM lattice structures: Properties, performance, applications and challenges. *Mater. Design* **2019**, *183*, 108137. [[CrossRef](#)]
27. Yang, C.; Zhang, C.; Chen, Z.J.; Li, Y.; Yan, W.Y.; Yu, H.B.; Liu, L. Three-dimensional hierarchical porous structures of metallic glass/copper composite catalysts by 3D printing for efficient wastewater treatments. *ACS Appl. Mater. Interfaces* **2021**, *13*, 7227–7237. [[CrossRef](#)]
28. Cai, C.; Guo, S.; Li, B.Y.; Tian, Y.J.; Qiu, J.C.D.; Sun, C.N.; Yan, C.Z.; Qi, H.J.; Zhou, K. 3D printing and chemical dealloying of a hierarchically micro-and nanoporous catalyst for wastewater purification. *ACS Appl. Mater. Interfaces* **2021**, *13*, 48709–48719. [[CrossRef](#)]

29. Zhang, L.; Fu, Y.S.; Wang, Z.R.; Zhou, G.F.; Zhou, R.Y.; Liu, Y.Q. Removal of diclofenac in water using peracetic acid activated by zero valent copper. *Sep. Purif. Technol.* **2021**, *276*, 119319. [[CrossRef](#)]
30. Zhu, F.; Li, L.; Ma, S.Y.; Shang, Z.F. Effect factors, kinetics and thermodynamics of remediation in the chromium contaminated soils by nanoscale zero valent Fe/Cu bimetallic particles. *Chem. Eng. J.* **2016**, *302*, 663–669. [[CrossRef](#)]
31. Zheng, Y.K.; Zhang, L.; Guan, J.; Qian, S.Y.; Zhang, Z.X.; Ngaw, C.K.; Wan, S.L.; Wang, S.; Lin, J.D.; Wang, Y. Controlled synthesis of Cu⁰/Cu₂O for efficient photothermal catalytic conversion of CO₂ and H₂O. *ACS Sustain. Chem. Eng.* **2021**, *9*, 1754–1761. [[CrossRef](#)]
32. Yang, Z.; Liu, Y.; Wang, J.L. MOF-derived Cu⁰/C activation of molecular oxygen for efficient degradation of sulfamethazine. *Chem. Eng. J.* **2022**, *427*, 131961. [[CrossRef](#)]
33. Shen, H.Y.; Sun, P.J.; Meng, X.; Wang, J.L.; Liu, H.Y.; Xu, L.J. Nanoscale Fe⁰/Cu⁰ bimetallic catalysts for Fenton-like oxidation of the mixture of nuclear-grade cationic and anionic exchange resins. *Chemosphere* **2021**, *269*, 128763. [[CrossRef](#)]
34. Kong, A.Q.; Ji, Y.H.; Ma, H.H.; Song, Y.F.; He, B.Q.; Li, J.X. A novel route for the removal of Cu(II) and Ni(II) ions via homogeneous adsorption by chitosan solution. *J. Clean. Prod.* **2018**, *192*, 801–808. [[CrossRef](#)]
35. Zhang, X.; Xu, B.K.; Wang, S.W.; Li, X.; Liu, B.M.; Xu, Y.H.; Yu, P.; Sun, Y.J. High-density dispersion of CuN_x sites for H₂O₂ activation toward enhanced photo-Fenton performance in antibiotic contaminant degradation. *J. Hazard. Mater.* **2022**, *423*, 127039. [[CrossRef](#)]
36. Wu, Z.Z.; Gu, Y.Y.; Xin, S.S.; Lu, L.L.; Huang, Z.W.; Li, M.Y.; Cui, Y.F.; Fu, R.B.; Wang, S.B. Cu_xNi_yCo-LDH nanosheets on graphene oxide: An efficient and stable Fenton-like catalyst for dual-mechanism degradation of tetracycline. *Chem. Eng. J.* **2022**, *434*, 134574. [[CrossRef](#)]
37. Liu, M.G.; Xia, H.; Yang, W.X.; Liu, X.Y.; Xiang, J.; Wang, X.M.; Hu, L.S.; Lu, F.S. Novel Cu-Fe bimetal oxide quantum dots coupled g-C₃N₄ nanosheets with H₂O₂ adsorption-activation trade-off for efficient photo-Fenton catalysis. *Appl. Catal. B—Environ.* **2022**, *301*, 120765. [[CrossRef](#)]
38. Huang, G.Y.; Chang, W.J.; Lu, T.W.; Tsai, I.L.; Wu, S.J.; Ho, M.H.; Mi, F.L. Electrospun CuS nanoparticles/chitosan nanofiber composites for visible and near-infrared light-driven catalytic degradation of antibiotic pollutants. *Chem. Eng. J.* **2022**, *431*, 134059. [[CrossRef](#)]
39. Ma, X.; Cheng, Y.Q.; Ge, Y.J.; Wu, H.D.; Li, Q.S.; Gao, N.Y.; Deng, J. Ultrasound-enhanced nanosized zero-valent copper activation of hydrogen peroxide for the degradation of norfloxacin. *Ultrason. Sonochem.* **2018**, *40*, 763–772. [[CrossRef](#)]
40. Lyu, L.; Cao, W.R.; Yu, G.F.; Yan, D.B.; Deng, K.L.; Lu, C.; Hu, C. Enhanced polarization of electron-poor/rich micro-centers over nZVCu-Cu(II)-rGO for pollutant removal with H₂O₂. *J. Hazard. Mater.* **2020**, *383*, 121182. [[CrossRef](#)]
41. Fang, Z.Y.; Zhao, J.; Li, Y.; Wang, Y.; Qiu, T.; Wu, Y.L.; Dong, W.B.; Mailhot, G. Improving Fenton-like system with catechin, an environmental-friendly polyphenol: Effects and mechanism. *Chem. Eng. J.* **2021**, *426*, 127946. [[CrossRef](#)]
42. Hou, L.W.; Wang, L.G.; Royer, S.; Zhang, H. Ultrasound-assisted heterogeneous Fenton-like degradation of tetracycline over a magnetite catalyst. *J. Hazard. Mater.* **2016**, *302*, 458–467. [[CrossRef](#)]
43. Guo, S.; Zhang, L.J.; Chen, M.; Ahmad, F.; Fida, H.; Zhang, H.L. Heterogeneous activation of peroxymonosulfate by a spinel CoAl₂O₄ catalyst for the degradation of organic pollutants. *Catalysts* **2022**, *12*, 847. [[CrossRef](#)]
44. Xu, L.J.; Yang, Y.J.; Li, W.Y.; Tao, Y.J.; Sui, Z.G.; Song, S.; Yang, J. Three-dimensional macroporous graphene-wrapped zero-valent copper nanoparticles as efficient micro-electrolysis-promoted Fenton-like catalysts for metronidazole removal. *Sci. Total Environ.* **2019**, *658*, 219–233. [[CrossRef](#)] [[PubMed](#)]
45. Zhou, C.; Gao, N.Y.; Deng, Y.; Chu, W.C.; Rong, W.L.; Zhou, S.D. Factors affecting ultraviolet irradiation/hydrogen peroxide (UV/H₂O₂) degradation of mixed n-nitrosamines in water. *J. Hazard. Mater.* **2012**, *231*, 43–48. [[CrossRef](#)]
46. Li, W.; Chen, C.; Zhu, J.Y.; Zhou, L.X.; Lan, Y.Q. Efficient removal of aniline by micro-scale zinc-copper (mZn/Cu) bimetallic particles in acidic solution: An oxidation degradation mechanism via radicals. *J. Hazard. Mater.* **2019**, *366*, 482–491. [[CrossRef](#)]
47. Yu, B.W.; Li, Z.J.; Zhang, S.L. Zero-valent copper-mediated peroxymonosulfate activation for efficient degradation of azo dye orange G. *Catalysts* **2022**, *12*, 700. [[CrossRef](#)]
48. Xu, Z.; Wu, Y.J.; Wang, X.; Ji, Q.Y.; Li, T.Z.; He, H.; Song, H.O.; Yang, S.G.; Li, S.Y.; Yan, S.C.; et al. Identifying the role of oxygen vacancy on cobalt-based perovskites towards peroxymonosulfate activation for efficient iohexol degradation. *Appl. Catal. B—Environ.* **2022**, *319*, 121901. [[CrossRef](#)]
49. Guo, S.; Yang, Z.X.; Zhang, H.L.; Yang, W.; Li, J.; Zhou, K. Enhanced photocatalytic degradation of organic contaminants over CaFe₂O₄ under visible LED light irradiation mediated by peroxymonosulfate. *J. Mater. Sci. Technol.* **2020**, *62*, 34–43. [[CrossRef](#)]
50. Guo, S.; Liu, M.D.; You, L.M.; Cheng, G.; Li, J.; Zhou, K. Oxygen vacancy induced peroxymonosulfate activation by Mg-doped Fe₂O₃ composites for advanced oxidation of organic pollutants. *Chemosphere* **2021**, *279*, 130482. [[CrossRef](#)]
51. Zhen, Y.F.; Sun, Z.Q.; Jia, Z.Y.; Liu, C.H.; Zhu, S.S.; Li, X.Y.; Wang, W.; Ma, J. Facile preparation of α-MnO₂ nanowires for assembling free-standing membrane with efficient Fenton-like catalytic activity. *Chin. Chem. Lett.* **2023**, *34*, 107664. [[CrossRef](#)]
52. Shi, J.G.; Ai, Z.H.; Zhang, L.Z. Fe@Fe₂O₃ core-shell nanowires enhanced Fenton oxidation by accelerating the Fe(III)/Fe(II) cycles. *Water Res.* **2014**, *59*, 145–153. [[CrossRef](#)]
53. Peng, W.; Niu, W.J.; Paerhati, S.; Guo, W.J.; Ma, J.G.; Hou, J.W. Facile synthesis of n-Fe₃O₄/ACF functional cathode for efficient dye degradation through heterogeneous E-Fenton process. *Catalysts* **2022**, *12*, 879. [[CrossRef](#)]
54. Katagi, T. Photodegradation of pesticides on plant and soil surfaces. *Rev. Environ. Contam. Toxicol.* **2004**, *182*, 1–78.

55. Qi, J.J.; Yang, X.Y.; Pan, P.Y.; Huang, T.B.; Yang, X.D.; Wang, C.C.; Liu, W. Interface engineering of $\text{Co}(\text{OH})_2$ nanosheets growing on the KNbO_3 perovskite based on electronic structure modulation for enhanced peroxymonosulfate activation. *Environ. Sci. Technol.* **2022**, *56*, 5200–5212. [[CrossRef](#)]
56. Sun, Y.; Tian, P.F.; Ding, D.D.; Yang, Z.X.; Wang, W.Z.; Xin, H.; Xu, J.; Han, Y.F. Revealing the active species of Cu-based catalysts for heterogeneous Fenton reaction. *Appl. Catal. B—Environ.* **2019**, *258*, 117985. [[CrossRef](#)]
57. Liu, T.C.; Yin, K.; Li, N.; Liu, H.; Chen, J.B.; Zhou, X.F.; Zhang, Y.L. Efficient activation of peroxymonosulfate by copper supported on polyurethane foam for contaminant degradation: Synergistic effect and mechanism. *Chem. Eng. J.* **2022**, *427*, 131741. [[CrossRef](#)]
58. Meng, S.; Zhou, P.; Sun, Y.M.; Zhang, P.; Zhou, C.Y.; Xiong, Z.K.; Zhang, H.; Liang, J.; Lai, B. Reducing agents enhanced Fenton-like oxidation (Fe (III)/Peroxydisulfate): Substrate specific reactivity of reactive oxygen species. *Water Res.* **2022**, *218*, 118412. [[CrossRef](#)]
59. Shah, N.S.; Khan, J.A.; Sayed, M.; Lqbal, J.; Khan, Z.U.H.; Muhammad, N.; Polychronopoulou, K.; Hussain, S.; Imran, M.; Murtaza, B.; et al. Nano-zero valent copper as a Fenton-like catalyst for the degradation of ciprofloxacin in aqueous solution. *J. Water Process Eng.* **2020**, *37*, 101325. [[CrossRef](#)]
60. Xu, Z.; Shan, C.; Xie, B.H.; Liu, Y.; Pan, B.C. Decomplexation of Cu(II)-EDTA by UV/persulfate and UV/ H_2O_2 : Efficiency and mechanism. *Appl. Catal. B—Environ.* **2017**, *200*, 439–447. [[CrossRef](#)]
61. Sun, L.; Jiang, H.; Zhao, Y.X.; Wan, J.; Li, L.L.; Wang, L.Y. Facile synthesis of copper-based bimetallic oxides for efficient removal of bisphenol A via Fenton-like degradation. *Sep. Purif. Technol.* **2021**, *279*, 119724.
62. Lin, C.C.; Zhong, Y.H. Performance of nZVC/ H_2O_2 process in degrading chloramphenicol in water. *J. Taiwan Inst. Chem. E.* **2021**, *129*, 112–117. [[CrossRef](#)]
63. Shen, M.X.; Huang, Z.J.; Luo, X.W.; Ma, Y.J.; Chen, C.Y.; Chen, X.; Cui, L.H. Activation of persulfate for tetracycline degradation using the catalyst regenerated from Fenton sludge containing heavy metal: Synergistic effect of Cu for catalysis. *Chem. Eng. J.* **2020**, *396*, 125238. [[CrossRef](#)]
64. Cui, Y.L.; Zheng, J.; Zhu, Z.J.; Hu, C.Y.; Liu, B.J. Preparation and application of $\text{Bi}_4\text{O}_7/\text{Cu-BiOCl}$ heterojunction photocatalyst for photocatalytic degradation of tetracycline under visible light. *J. Mol. Struct.* **2023**, *1274*, 134486. [[CrossRef](#)]
65. Li, B.S.; Lai, C.; Xu, P.; Zeng, G.M.; Huang, D.L.; Qiu, L.; Yi, H.; Cheng, M.; Wang, L.L.; Huang, F.L.; et al. Facile synthesis of bismuth oxyhalogen-based Z-scheme photocatalyst for visible-light-driven pollutant removal: Kinetics, degradation pathways and mechanism. *J. Clean. Prod.* **2019**, *225*, 898–912. [[CrossRef](#)]
66. Sun, S.S.; Teng, Q.; Xie, Y.; Liu, T.; Ma, R.; Bai, J.; Cai, C.; Wei, Q.S. Two-step heat treatment for laser powder bed fusion of a nickel-based superalloy with simultaneously enhanced tensile strength and ductility. *Addit. Manuf.* **2021**, *46*, 102168. [[CrossRef](#)]

Disclaimer/Publisher’s Note: The statements, opinions and data contained in all publications are solely those of the individual author(s) and contributor(s) and not of MDPI and/or the editor(s). MDPI and/or the editor(s) disclaim responsibility for any injury to people or property resulting from any ideas, methods, instructions or products referred to in the content.